6

A Novel Traction Control for Electric Vehicle without Chassis Velocity

Dejun Yin and Yoichi Hori
University of Tokyo
Japan

1. Introduction

Due to the growing concern about global environmental problems and shrinking non-renewable energy sources, research on electric vehicles and hybrid electric vehicles is once again attracting significant attention. Meanwhile, significant improvements in power electronics, energy storage and control technology have made electric vehicles fully feasible, preparing the state of the art for their return to the market (Chau et al., 2008; Affanni et al., 2005; Nagai, 2007).

Beside the advantages for the environment, manufacture and maintenance, from the viewpoint of control technology, the most distinct advantages of electric vehicles have not been well recognized. Since electric vehicles and some specially configured hybrid electric vehicles are driven by electric motors, the advantages provided to these electric vehicles can be summarized as follows (Hori, 2004):

1. Quick torque generation
2. Easy torque measurement
3. Possibility of independently equipped motors for each wheel

On the other hand, considering the different regions of the world, the increase of the mobility shows a clear correlation to the gross domestic product. With further economic growth, we can predict an even greater increase in mobility and in traffic density throughout the world. For this reason, vehicle motion control systems have been developed to provide active safety control, and have made significant technological progress over the last decade to enhance vehicle stability and handling performance in critical dynamic situations by introducing computer control technology.

From the development history of vehicle motion control, it can also be found that, effective operation of any vehicle control system is based on some basic assumptions, for example, the output torque being able to accurately work on the vehicle. For this purpose, traction control, as the most primary active safety control for vehicles, is developed to ensure the effectiveness of the torque output. The key to traction control is antislip control, when the vehicle is driven or brakes on a slippery road, especially for light vehicles because they are more inclined to skid on slippery roads. Traction control must not only guarantee the effectiveness of the torque output to maintain vehicle stability, but also provide some information about tire-road conditions to other vehicle control systems. Moreover, in electric vehicles a well-managed traction control system can cover the functions of ABS, because

Source: Motion Control, Book edited by: Federico Casolo,
ISBN 978-953-7619-55-8, pp. 580, January 2010, INTECH, Croatia, downloaded from SCIYO.COM

electric motors can generate deceleration torque as easily as acceleration torque (Mutoh et al., 2007). Based on the core traction control, more complicated two-degree-of-freedom motion control for vehicles can be synthesized by introduction of some additional information on steering angle, yaw rate, lateral acceleration and so on (Saito et al., 2002; Fujimoto et al., 2004). Moreover, from the viewpoint of the relation between safety and cost, a more advanced traction control synthesis also means lower energy consumption.

However, actual vehicles present challenges to research on traction control. For example, the real chassis velocity is not available, and the friction force that it is to drives the vehicle is immeasurable in real time. Conventional traction control in internal combustion engine vehicles, according to nonlinear tire models such as the Magic Formula (Pacejka & Bakker, 1992), has to calculate the chassis velocity and the slip ratio to acquire maximum friction force from the road. For this purpose, due to physical and economic reasons, the non-driven wheels are usually utilized to provide an approximate vehicle velocity. However, this method is not applicable when the vehicle is accelerated by 4WD systems or decelerated by brakes equipped in these wheels. For this reason, the accelerometer measurement is also used to calculate the velocity value, but it cannot avoid offset and error problems. Other sensors, e.g., optical sensors (Turner & Austin, 2000), sensors of magnetic markers (Lee & Tomizuka, 2003; Suryanarayanan & Tomizuka, 2007), etc., can also obtain the chassis velocity. However, they are too sensitive and reliant on the driving environment or too expensive to be applied in actual vehicles.

In order to overcome the obstacles of calculating chassis velocity, some controllers in electric vehicles, for example Model Following Control (MFC), do not need information on chassis velocity or even acceleration sensors. In these systems, the controllers only make use of torque and wheel rotation as input variables for calculation. Fewer sensors contribute not only to lower cost, but also higher reliability and greater independence from driving conditions, which are the most outstanding merits of this class of control systems. Accordingly, research on more practical and more sophisticated antislip control based on MFC continues until now. Sakai et al. proposed a primary MFC system for antislip control (Sakai & Hori, 2001). Saito et al. modified it and proposed a novel stability analysis to determine the maximum feedback gain, and furthermore, used the antislip control as a core subsystem and extended it to two-degree-of-freedom motion control (Saito et al., 2002; Fujimoto et al., 2004). Akiba et al. improved the control performance by introduction of back electromotive force, and added a conditional limiter to avoid some of its inherent drawbacks (Akiba et al., 2007). Nevertheless, these control designs based on compensation have to consider the worst stability case to decide the compensation gain, which impairs the performance of antislip control. Furthermore, gain tuning for some specific tire-road conditions also limits the practicability of this method.

Therefore, this work, making use of the advantages of electric vehicles, focuses on development of a core traction control system based on Maximum Transmissible Torque Estimation (MTTE) which requires neither chassis velocity nor information about tire-road conditions. In this system, use is made of only the torque reference and the wheel rotation to estimate the maximum transmissible torque to the road surface, then the estimated torque is applied for antislip control implementation. Moreover, the proposed control method is expected to provide a general approach for traction control, as well as a basis for more complicated and advanced motion control in electric vehicles.

The rest of the paper is structured as follows. A novel topology of traction control, based on the proposed maximum transmissible torque estimation, is presented in Section 2, and an equivalent model is used to provide the stability analysis of the control system. Section 3

discusses the experimental electric vehicle and presents the experimental results, as well as additional simulation results. These comparative results are followed by a detailed discussion including stability, control performance and robustness in Section 4.

2. Maximum transmissible torque estimation for antislip control

2.1 Longitudinal model and dynamic analysis

Because only longitudinal motion is discussed in this paper, the dynamic longitudinal model of the vehicle can be described as in Fig. 1 and the parameter definition is listed in Table 1. Generally, the dynamic differential equations for the calculation of longitudinal motion of the vehicle are described as follows:

$$J_w\dot{\omega} = T - rF_d \tag{1}$$

$$M\dot{V} = F_d - F_{dr} \tag{2}$$

$$V_w = r\omega \tag{3}$$

$$F_d(\lambda) = \mu N \tag{4}$$

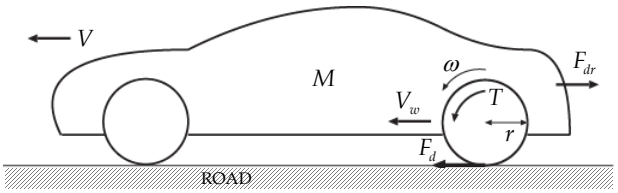

Fig. 1. Dynamic longitudinal model of the vehicle

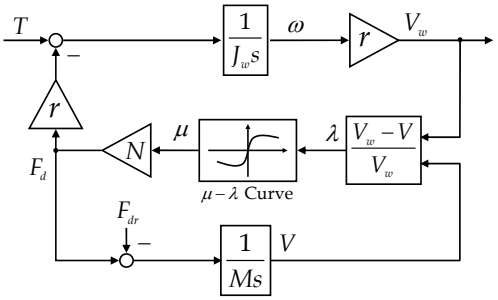

Fig. 2. One-wheel vehicle model with Magic Formula.

The interrelationships between the slip ratio and friction coefficient can be described by various formulas. Here, as shown in Fig. 2, the widely adopted Magic Formula is applied to build a vehicle model for the following simulations. The slip ratio in (4) is defined as (5). Fig. 3 describes a typical relationship between slip ratio and friction coefficient.

$$\lambda = \frac{V_w - V_x}{\max(V_w, V_x)} \tag{5}$$

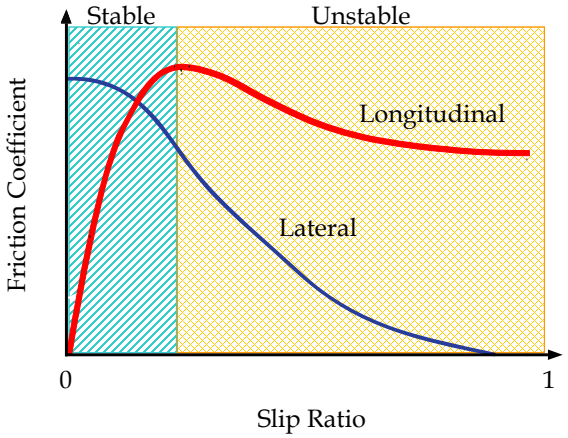

Fig. 3. A typical $\mu - \lambda$ curve

2.2 Maximum transmissible torque estimation

In this work, in order to avoid the complicated μ - λ relation, only the dynamic relation between tire and chassis is considered based on the following considerations, which transform the antislip control into maximum transmissible torque control.

1. Whatever kind of tire-road condition the vehicle is driven in, the kinematic relationship between the wheel and the chassis is always fixed and known. Although this relationship also exists in the dynamics of an internal combustion engine vehicle, it is very difficult to realize this consideration in these vehicles. However, the rigidity of an electric motor makes this possible.
2. During the acceleration phase, considering stability and tire abrasion, well-managed control of the velocity difference between wheel and chassis is more important than the mere pursuit of absolute maximum acceleration.
3. If the wheel and the chassis accelerations are well controlled, the difference between the wheel and the chassis velocities, i.e. the slip, is also well controlled.

According to (1) and (3), the driving force, i.e. the friction force between the tire and the road surface, can be calculated as (6). Assuming T is constant, it can be found that the higher V_w, the lower F_d. In normal road conditions, F_d is less than the maximum friction force from the road and increases as T goes up. However, when slip occurs, F_d will become smaller than the maximum friction force that the tire-road relation can provide and cannot increase with T. Here, there are only two parameters, r and J_w, so F_d is easily calculated in most tire-road conditions.

$$F_d = \frac{T - J_w \dot{\omega}}{r} \tag{6}$$

When slip starts to occur, the difference between the velocities of the wheel and the chassis becomes larger and larger, i.e. the acceleration of the wheel is larger than that of the chassis. Furthermore, according to the Magic Formula, the difference between the accelerations will make the slip more severe.

Symbol	Definition
J_w	Wheel Inertia
V_w	Wheel Velocity (Circumferential Velocity)
ω	Wheel Rotation
T	Driving Torque
r	Wheel Radius
F_d	Friction Force (Driving Force)
M	Vehicle Mass
N	Vehicle Weight
V	Chassis Velocity (Vehicle Velocity)
F_{dr}	Driving Resistance
λ	Slip Ratio
μ	Friction Coefficient

Table 1. Parameter list

Therefore, the condition that the slip does not start or become more severe is that the acceleration of the wheel is close to that of the chassis. Moreover, considering the μ - λ relation described in the Magic Formula, an appropriate difference between chassis velocity and wheel velocity is necessary to provide the friction force. Accordingly, (7) defines a as a relaxation factor to describe the approximation between the accelerations of the chassis and the wheel. In order to satisfy the condition that slip does not occur or become larger, a should be close to one.

$$\alpha = \frac{\dot{V}^*}{\dot{V}_w^*}, \text{ i.e. } \alpha = \frac{(F_d - F_{dr})/M}{(T_{\max} - rF_d)r/J_w} \tag{7}$$

With a designed a, when the vehicle enters a slippery road, $T_{\max}$ must be reduced adaptively following the decrease of F_d to satisfy (7), the no-slip condition.

Since the friction force from the road is available from (6), the maximum transmissible torque, $T_{\max}$ can be calculated as (8). This formula indicates that a given F_d allows a certain maximum torque output from the wheel so as not to increase the slip. Here, it must be pointed out that driving resistance, F_{dr}, is assumed to be zero, which will result in an over evaluation of $T_{\max}$ and consequently impair the anti-slip performance. However, F_{dr} is a variable related with the chassis velocity and the vehicle shape, and can be calculated or estimated in real time if higher anti-slip performance is required or if the vehicle runs at high speed (Sakai et al., 1999; Cao et al., 2006). Although the vehicle mass, M can also be estimated online (Ikeda et al., 1992; Winstead & Kolmanovsky, 2005; Phornsuk et al., 2006), in this paper it is assumed to be constant. Due to these assumptions, the following sections will evaluate and analyze the robustness to disturbances in driving resistance and the perturbation in vehicle mass.

$$T_{\max} = \left(\frac{J_w}{\alpha M r^2} + 1 \right) r F_d \tag{8}$$

Finally, the proposed controller can use $T_{\max}$ to constrain the torque reference if necessary.

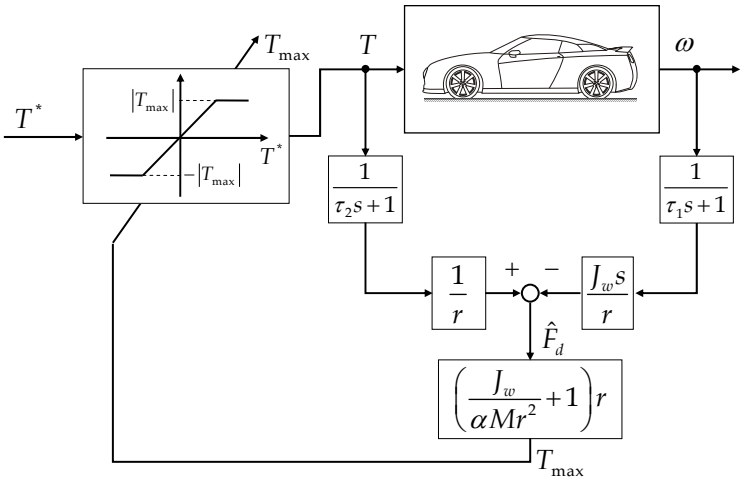

Fig. 4. Primary control system based on MTTE

2.3 Controller design

The torque controller is designed as in Fig. 4, in which the limiter with a variable saturation value is expected to realize the control of torque output according to the dynamic situation. Under normal conditions, the torque reference is expected to pass through the controller without any effect. On the other hand, when on a slippery road, the controller can constrain the torque output to be close to $T_{\max}$.

Firstly, the estimator uses the driving torque generated by the motor and the rotation speed of the wheel to calculate the friction force, and then estimates the maximum transmissible torque according to (8). Finally, the controller utilizes the estimated torque value as a saturation value to limit the commanded torque, T^*. In essence, the estimation shown in Fig. 4 is a disturbance observer.

Here, although it will cause some phase shift, duo to the low resolution of the shaft encoder installed in the wheel, a low pass filter (LPF) with a time constant of τ_1 is introduced to smooth the digital signal, ω, for the differentiator which follows. In order to keep the filtered signals in phase, another LPF with a time constant of τ_2 is added for T.

In the actual controllers, the wheel radius, r, in the blocks can be combined to reduce the calculations.

2.4 Stability analysis

Considering that the Magic Formula included in the vehicle model shown in Fig. 2 is non-linear, this work makes use of an equivalent model for stability analysis to decide on parameters.

Slip occurs when part of the outputted torque cannot be transmitted to the chassis by the tire-road interaction, resulting in lower chassis acceleration than that of wheel. Here, (9) uses Δ to describe the ratio of the under-transmitted torque.

In addition, taking into account the ideal state and the worst-case slip in which the wheel spins completely idly, that is, the inertia of the whole system is equal to the inertia of wheel, J_w, the variation range of Δ, as (10), is available too.

$$\dot{V} - \dot{V}_w = -\frac{\Delta T}{Mr} \tag{9}$$

$$\Delta \in [0,\ Mr^2/J_w] \tag{10}$$

According to (1), (2) and (9), the dynamic longitudinal model of the vehicle can be simplified as in (11), a Single-Input-Single-Output system which masks the complicated interaction among tire, chassis and road, which contributes to the stability analysis. That is, the unwanted wheel acceleration that causes slip can be regarded as the result of a decrease in system inertia. And, Δ can also be treated as a description of variation in system inertia.

$$J\dot{\omega} = T \tag{11}$$

Here, as shown in (12), J is the equivalent inertia of the whole vehicle system from the viewpoint of the driving wheel, and J_n the nominal inertia where no slip occurs.

$$J = \frac{J_n}{1+\Delta},\ J_n = J_w + Mr^2 \tag{12}$$

Consequently, use is made of (12) to take place of the vehicle model shown in Fig. 4 for stability analysis. When the vehicle rapidly accelerates on a slippery road, the estimated $T_{\max}$ will constrain T^* and take its place to be treated as the input value to the motor. In this case, the whole system will automatically transform into a closed feedback system, as shown in Fig. 5.

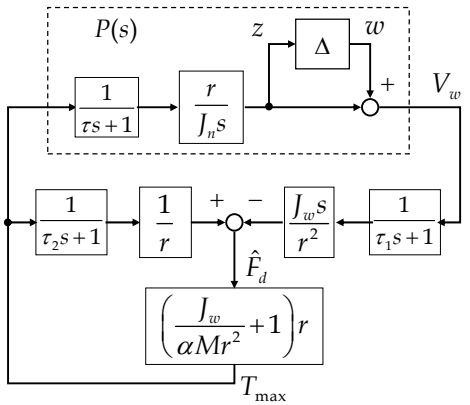

Fig. 5. Equivalent closed-loop control system

Here, in order to analyze the stability easily, the delay of the electro-mechanical system is simplified as a LPF with a time constant of τ. However, in the following simulation, according to the behaviour of real vehicle, the system delay is simulated by a pure delay and a LPF.

The system of Fig. 6, which is the equivalent block diagram of Fig. 5, is used for the analysis of the closed-loop stability against Δ, the model variation. T_{zw}, the transfer function from w to z in Fig. 6, is described in (13).

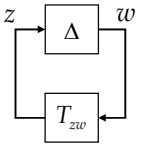

Fig. 6. Equivalent block diagram for stability analysis

$$T_{zw} = \frac{-J_w K}{J_n r\tau\tau_1 s^2 + J_n((r-K)\tau + r\tau_1)s + J_n r - Mr^2 K} \tag{13}$$

Here,

$$K = \left(\frac{J_w}{\alpha M r^2} + 1\right) r \tag{14}$$

As a result, the following conditions in (16) must be satisfied to ensure the closed-loop stability, that is, ensure the real part of the roots of the characteristic equation, (15), to be negative (Ioannou & Sun, 1995). Here, τ_2 is assumed equal to τ_1 to simplify the solution.

$$1 - T_{zw}\Delta = 0 \tag{15}$$

$$\begin{cases} \alpha > \dfrac{1 - J_w \Delta / M r^2}{1 + \Delta} \\ \tau_1 > \dfrac{J_w \tau}{\alpha M r^2} \end{cases} \tag{16}$$

It can be found in (16) that if there is no limiter, when the vehicle runs in a normal state, a must be larger than 1 to fulfil the requirement for stability. However, considering (8), when a is larger than one, $T_{\max}$ will be always restrained to be smaller than the torque that the tire-road interface can provide, which will impair the acceleration performance. Therefore, in this work, a is designed to be slightly smaller than one to ensure acceleration performance while improving the antislip performance.

2.5 Compensation for acceleration performance

In real experiments, even in normal road conditions, $T_{\max}$ may be smaller than T^* due to system delay at the acceleration start, which will cause suddenly commanded acceleration to be temporarily constrained by $T_{\max}$ during the acceleration phase.

In order to avoid this problem, the increasing rate of T^* is amplified as a stimulation to force the under-evaluated $T_{\max}$ to the acceleration reference. $T'_{\max}$ is used instead of $T_{\max}$ as the input to the controller, whose relation is described by (17). Here, G is a compensation gain. Additionally, the over-expanded $T'_{\max}$ can be automatically constrained by the following controller.

$$T'_{\max} = T_{\max} + \dot{T}^* G \ (\dot{T}^* > 0) \tag{17}$$

The value of G should be decided corresponding to the total delay in the system and the maximum acceleration rate that the vehicle permits. Generally, larger delay or a higher acceleration rate requires a larger value for G.

Fig. 7. COMS3 - a new experimental electric vehicle

3. Experiments and simulation

3.1 Experimental electric vehicle

In order to implement and verify the proposed control system, a commercial electric vehicle, COMS, which is made by TOYOTA AUTO BODY Co. Ltd., shown in Fig. 7 was modified to fulfil the experiments' requirements. Each rear wheel is equipped with an Interior Permanent Magnet Synchronous Motor (IPMSM) and can be controlled independently after modification.

As illustrated in Fig. 8, a control computer is added to take the place of the previous ECU to operate the motion control. The computer receives the acceleration reference signal from the acceleration pedal sensor, the forward/backward signal from the shift switch and the wheel rotation from the inverter. Then, the calculated torque reference of the left and the right rear wheel are independently sent to the inverter by two analog signal lines. Table 2 lists the main specifications of the experimental electric vehicle.

3.2 Experiments

Based on the algorithm shown in Fig. 4, the controllers were synthesized and discretized, and then implemented to COMS3 for experiments.

In these experiments, the slippery road was simulated by an acrylic sheet with a length of 1.2 m and lubricated with water. However, in all of the experiments, the friction coefficient between the tire and road surface was not measured and was unknown.

The initial velocity of the vehicle was set higher than 1 m/s to avoid the immeasurable zone of the shaft sensors installed in the wheels. However, the results of some additional experiments which were not included in this dissertation proved that the proposed control algorithm can also work when the vehicle starts off on a slippery road. In the comparative experiments, the initial velocities were kept to the same value as much as possible.

Here, it must be pointed out that in order to detect the chassis velocity and avoid mounting additional sensors for the experiment, only the left rear wheel is driven by the motor, while the right rear wheel rolls freely to provide a reference value of the chassis velocity for comparison. Due to the short track and small torque, the yaw moment resulting from the difference of torque between the left and the right wheels was too small to affect the

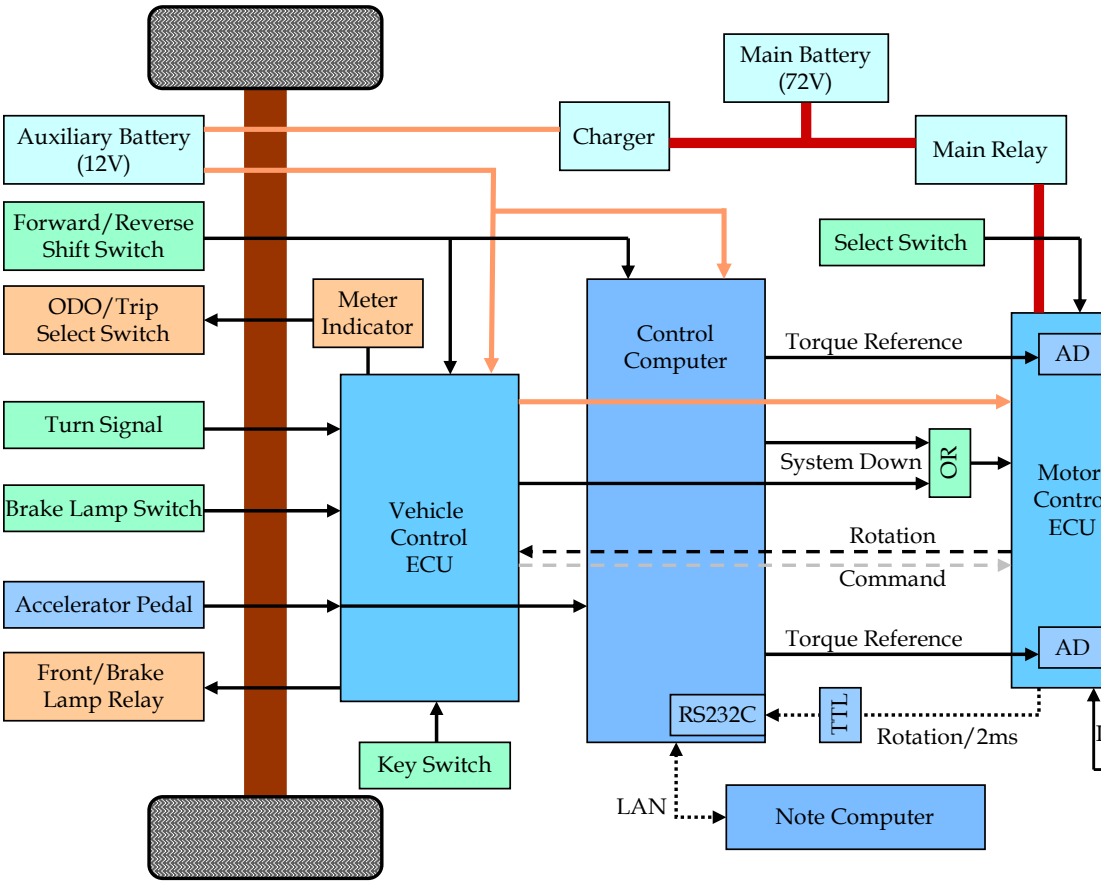
Main Battery
(72V)
Auxiliary Battery
(12V)
Charger
Main Relay
Forward/Reverse
Shift Switch
Select Switch
ODO/Trip
Select Switch
Meter
Indicator
Control
Computer
Torque Reference
AD
Turn Signal
System Down
OR
Brake Lamp Switch
Vehicle
Control
ECU
Motor
Contro
ECU
Rotation
Command
Accelerator Pedal
Torque Reference
AD
Front/Brake
Lamp Relay
RS232C
TTL
Rotation/2ms
Key Switch
LAN
Note Computer

Total Weight	360 kg
Max. Power	2000 W × 2
Max. Torque	100 Nm × 2
Wheel Inertia	0.5 kgm2 × 2
Wheel Radius	0.22 m
Sampling Time	0.01 s
Controller	PentiumM 1.8G, 1 GB RAM
A/D and D/A	12 bit
Shaft Encoder	36 pulse/round

Table 2. Specification of COMS3

experiments. Furthermore, this experimental method makes the vehicle skid more easily on the simulated slippery road.

In the following experiments where the robustness to disturbances in driving resistance was evaluated, the vehicle was attached to concrete blocks that were connected in a chain and dragged along the road to simulate the driving resistance due to wind or an uphill slope. The simulated driving resistance was measured by a dynamometer.

Fig. 9 describes the comparison of control performance between the control based on MTTE and MFC, as well as the non-control case.

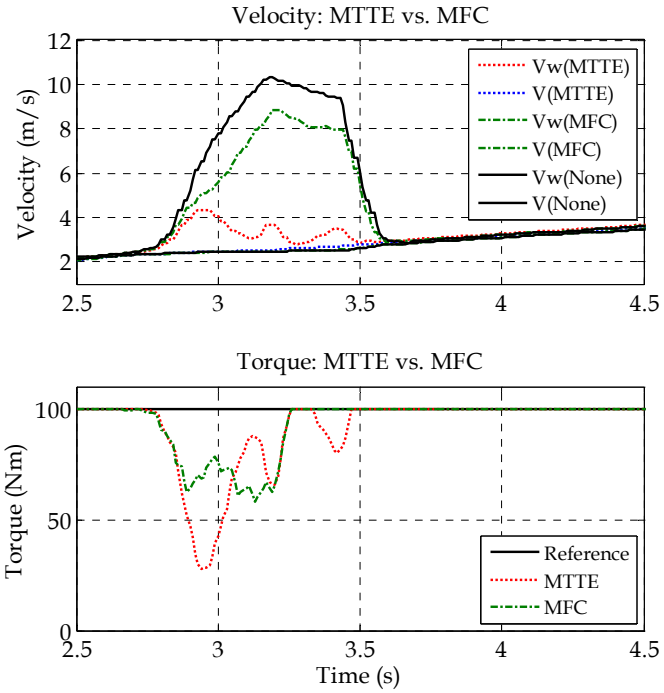

Fig. 9. Comparison of experimental results of two control designs

Because the vehicle mass varies significantly in a real driving environment, In order to evaluate the robustness to variation in vehicle mass, some comparative experiments were performed with different nominal mass in the proposed controller while keeping the real vehicle mass fixed at 360 kg. Fig. 10 provides these comparative results, in which the nominal mass varied from 180 kg to 360 kg.
Fig. 11 describes the results of the experiment with driving resistance. In these experiments, the driving resistance was simulated at 230 N, corresponding to the air resistance of a BMW 8-series running at a speed of 86 km/h.

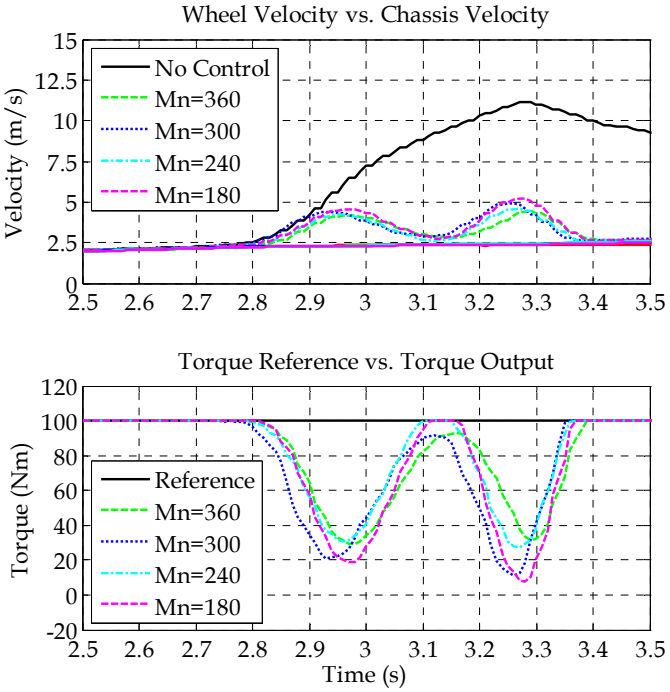

Fig. 10. Comparison of experimental results with variation in vehicle mass

3.2 Simulation

Due to the limitation of experimental equipment and facilities, the existing experimental results could not provide a comprehensive comparative demonstration to sufficiently reflect the features and essence of the proposed control topology. Therefore, numerical simulations were performed to provide more detailed comparisons and analysis, in which parameters could be set more precisely, providing finer insight into the controller behaviour than is possible through experiments alone. The following analysis and discussion will based on the experimental results, as well as on the simulation results.
Simulation systems were synthesized based on the algorithm in Fig. 4 and the vehicle model in Fig. 2. Here, it is must pointed that, in the vehicle model, a LPF with a time constant of 1 ms is placed after the friction coefficient to simulate the dynamics of the tire. The time constant is linearly related to the softness of the tire.

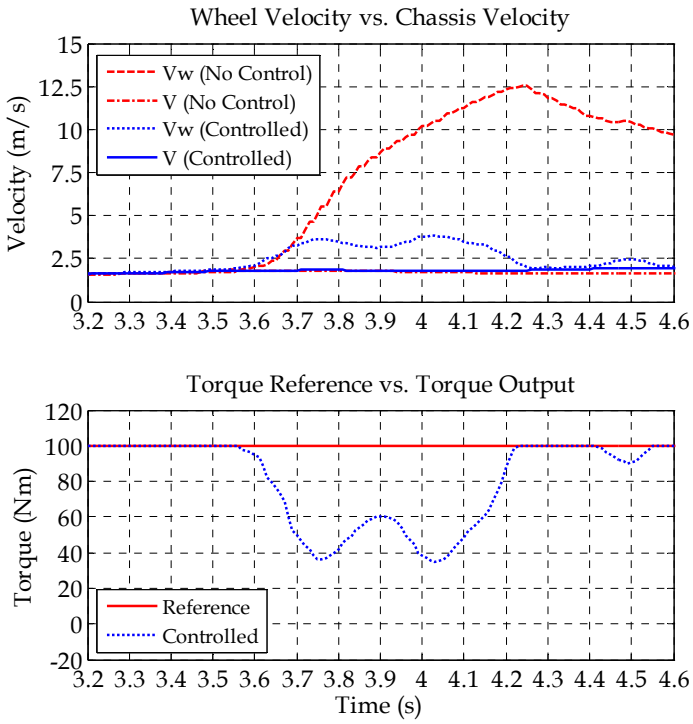

Fig. 11. Comparison of experimental results with driving resistance of 230 N

Fig. 12 illustrates the stability of the control system in which a is designed to be 0.9 for two different slip states. In these simulations, the system delay and time constants in LPFs are shortened to make the primary tendency clear. Here, system delay was set to 0, and time constants in the LPFs were set to 20 ms. In the simulation of severe slip, the maximum friction coefficient is set to 0.3, and a slight slip of 0.6. Here, the commonly used λ and Δ values are utilized to describe the extent of slip.

4. Discussion

4.1 Stability analysis

When a is smaller than one, according to (1) and (8), it can be found that when the vehicle runs in no-slip conditions, as described as (18), $T_{\max}$ will be larger than T^*, and the unwanted torque will be eliminated by the limiter, which keeps the system stable and responsive to the driver's torque reference. In this case, the torque reference from the driver passes through the controller and enters the motor, which makes the whole system operate like an open-loop control system.

$$T_{\max} = T + \frac{J_w}{r}\left(\frac{1}{\alpha}\dot{V} - \dot{V}_w\right) \tag{18}$$

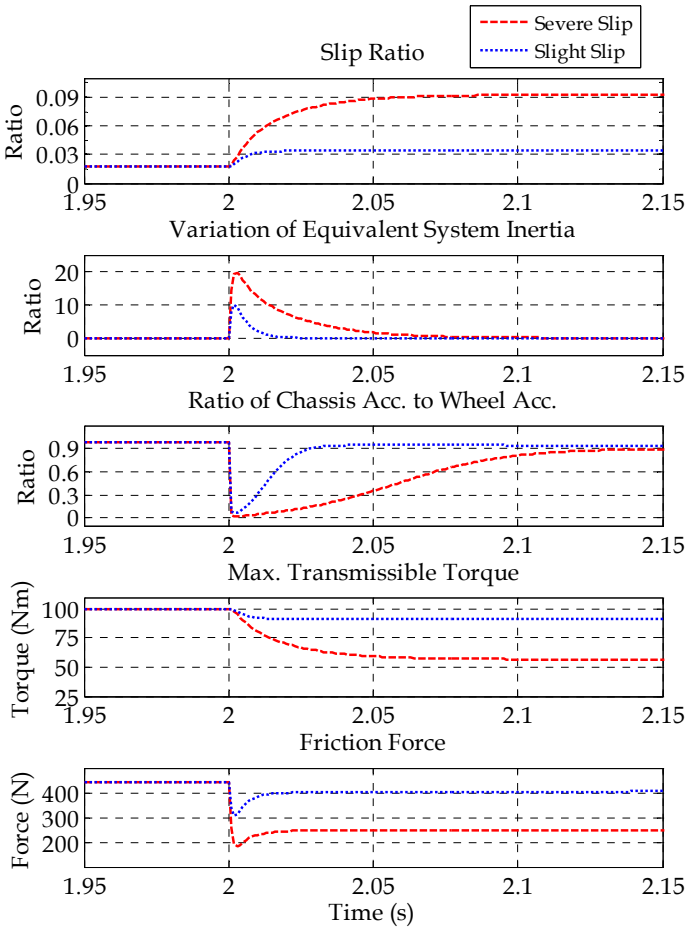

Fig. 12. System stability in different slippery conditions

On the other hand, when the vehicle enters a slippery road, as described in Fig. 12, due to the system delay, a sudden slip will occur at the first, and then, the whole system will work in two different states:

1. Slight slip that makes (16) valid, that is, the system is theoretically unstable. Therefore, at this time, the difference between the accelerations of the wheel and the chassis is in an expanding state, and this state will last until the ratio of the acceleration of the chassis to that of the wheel arrives at the designed value, a. However, a well designed a will allow T_{max} to rise to increase the slip properly, according to the Magic Formula, so as to provide an increased friction force, as expected.
2. Severe slip that satisfies (16) occurs. The system is stable, that is, T_{max} will become smaller and smaller to restrain the slip. The ratio of the acceleration of the chassis to that of the wheel will become larger and larger to meet the designed a.

In conclusion, the simulations and experiments indicate that, a relaxation factor a which is smaller than 1 makes the system work in a critical state, which results in the best antislip performance while keeping the system stable.

4.2 Control performance

Fig. 9 also shows that compared to the no-control case, the difference between the wheel velocity and the chassis velocity caused mainly by the delay in the control system does not increase. The estimated maximum transmissible torque is close to the input reference torque in the normal road, and corresponds to the maximum friction force allowed by the slippery tire-road surface. Moreover, the comparison with the control based on MFC demonstrated this control performance furthermore (Yin et al., 2009).

Perturbations in vehicle mass and the disturbances in driving resistance are usually the most uncertain factors in real driving environments. Fig. 10 and Fig. 11 show that the proposed control system has high robustness to perturbations in vehicle mass and disturbances in driving resistance.

4.3 Theoretical analysis with partially linearized model

Detailed analysis of control characteristics can be performed with a partially linearized vehicle model. When the control system operates in the closed-loop control state, if only the basic fact that the friction coefficient decreases with the velocity difference between the wheel and chassis is considered, the whole controlled system can be simplified as in Fig. 13.

Note that when the vehicle accelerates in a normal condition, that is, the friction force increases with the slip, considering the nonlinear tire model, in this model K_u should be a varying negative value. However, K_u is partially assumed to be positive, because the following discussion is limited to the condition where the slip ratio is in the unstable area as shown in Fig. 3.

In Fig. 13, F_{do} is the friction force between the tire and road surface when antislip control starts. M_n denotes the nominal vehicle mass and generally it is equal to the mass of the vehicle and the driver. Here, in order to simplify the analysis, the delay in the vehicle system is ignored and τ_2 is assumed to be equal to τ_1. Differentiation of the difference between the velocities is introduced due to the integral relation between the forces and the velocities.

The transfer function from F_{do} to A_D, and the one from F_{dr} to A_D can be defined as T_{Ad} and T_{Ar} respectively, in which J is the equivalent system inertia.

$$J = J_w + Mr^2 \tag{19}$$

$$T_{Ad} = \frac{-J\tau_1 s^2 + \left(\frac{M}{\alpha M_n} - 1\right) J_w s}{MJ_w\tau_1 s^2 + \left(MJ_w - JK_u\tau_1\right)s + \left(\frac{M}{\alpha M_n} - 1\right) J_w K_u} \tag{20}$$

$$T_{Ar} = \frac{J_w\tau_1 s^2 + J_w s}{MJ_w\tau_1 s^2 + \left(MJ_w - JK_u\tau_1\right)s + \left(\frac{M}{\alpha M_n} - 1\right) J_w K_u} \tag{21}$$

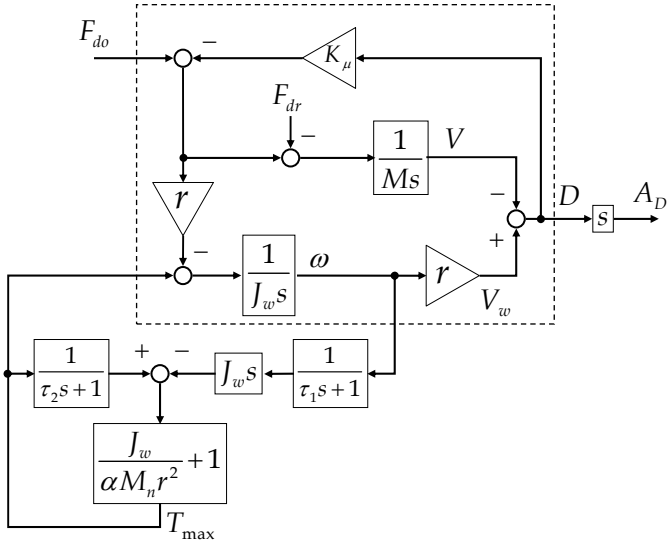

Fig. 13. Partially linearized control system

Here, Equation (20) is used as an example to examine the relation between the friction force and the differential of the velocity difference as follows.

$$\begin{aligned}\lim_{t\to\infty}\frac{A_D(t)}{F_{do}(t)} &= \lim_{s\to 0} T_{Ad}(s)\\ &< \lim_{s\to 0}\frac{-J\tau_1 s^2+\left(\frac{M}{\alpha M_n}-1\right)J_w s}{MJ_w\tau_1 s^2+\left(MJ_w-JK_u\tau_1\right)s}\\ &= \frac{\frac{M}{\alpha M_n}-1}{MJ_w-JK_u\tau_1}J_w\end{aligned} \tag{22}$$

Equation (22) shows that the differential of the slip is proportional to the friction force, which agrees with the additional simulation results shown in Fig. 14, in which small time constants in LPFs and small delay in the electromechanical system were adopted to examine the relation between the friction force and the velocity difference, a was set to 0.5, and the velocity difference representing the extent of the slip is equal to the difference between the wheel velocity and chassis velocity.

Equation (22) also indicates that when τ_1 or K_u is considerably larger, that is, the system delay causes the controller to be unable to follow the quickly varying friction force, the slip will become larger. Here, F_{do} is assumed to be a unit step reference.

4.4 Applied for two-degree-of-freedom motion control

From the viewpoint of the object of control, in the traction control based on MFC, the nominal model in the observer is the whole vehicle which varies drastically when the

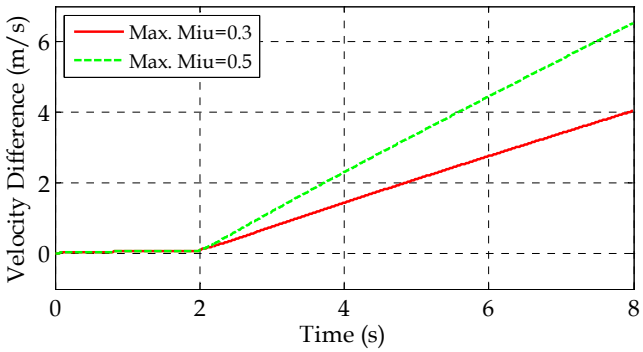

Fig. 14. Comparison of simulation results in different roads with small time constants

vehicle mass changes or load transfer among the driving wheels occurs during acceleration, braking or when the vehicle enters a curve. Therefore, this type of control method can be thought of as a control for the chassis behavior, which introduces the possibility that this control will interfere with other chassis control systems.

In contrast to this, the proposed control method is essentially based on control of wheel behavior rather than control of the whole chassis behavior, which decreases the interference with chassis controls, and also provides a sound independent basis for them.

Here, this work presents an example to demonstrate the application of the proposed traction control to planar motion control of electric vehicles. Fig. 15 shows the architecture of a Direct Yaw Moment Control enhanced by MTTE. Here, the steering-wheel angle, the estimated vehicle linear velocity and friction coefficient are used to calculate the nominal yaw rate, then the difference between the measured yaw velocity and the nominal yaw rate acts as the input to the traction distribution module. Finally, the traction distribution module generates the nominal torque reference for the MTTE.

5. Conclusion

This work proposed an estimator of maximum transmissible torque and applied it to the control of the driving motors in electric vehicles for slip prevention. This estimator, which does not calculate chassis velocity, instead using only the input torque and output rotation of the wheel, provides a good foundation for antislip control. The effectiveness of the estimation demonstrated that motors can act not only as actuators but also as a good platform for state estimation because of their inherently fast and accurate torque response. The experiments and simulations verified the effectiveness of the estimation in antislip control. Additionally, this estimator is also expected to provide the maximum transmissible torque for other vehicle control systems to enhance their control performance when the vehicle runs in slippery conditions.

The controller designed to co-operate with the estimator can provide higher antislip performance while maintaining control stability. When excessive torque is commanded, this controller constrains the control output to follow the actual maximum driving force between the tire and the road surface to prevent slip. In addition, the acceleration compensation resolved the problem of deterioration of pedal response due to system delay.

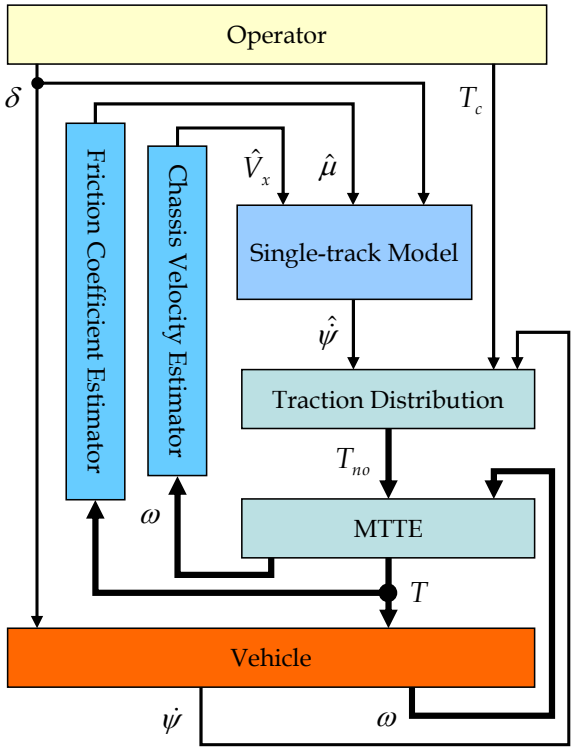

Fig. 15. A DYC system based on MTTE

Comparative experiments and simulations with variation of control variables and road conditions demonstrated the advantages of the proposed control design. The proposed control not only has a better antislip performance and higher adaptability in different tire-road conditions, but also has greater robustness to perturbations in vehicle mass and disturbances in driving resistance. These features enhance the applicability and practicality of this method. Furthermore, the detailed discussion and analysis on the experiments and simulations agreed with above evaluations and provided theoretical support for the proposed control topology. These advantages qualify the proposed control method as a general approach for traction control, as well as a basis for more sophisticated and advanced motion control in electric vehicles.

6. References

Affanni, A; Bellini, A; Franceschini, G; Guglielmi, P; & Tassoni, C. (2005). Battery Choice and Management for New-Generation Electric Vehicles, IEEE Transaction on Industrial Electronics, Vol. 52, No. 5, pp. 1343-1349.

Akiba, T.; Shirato, R.; Fujita, T. & Tamura, J. (2007). A study of Novel Traction Control Model for Electric Motor Driven Vehicle, Proceeding of 4th Power Conversion Conference-NAGOYA, pp. 699-704.

Cao, J. Y.; Cao, B. G. & Liu, Z. (2006). Driving Resistance Estimation Based on Unknown Input Observer, Journal of Applied Sciences, pp. 888-891.

Chau, K. T.; Chan, C. C. & Liu, C. (2008). Overview of Permanent-Magnet Brushless Drives for Electric and Hybrid Electric Vehicles, IEEE Transaction on Industrial Electronics, Vol. 55, No. 6, pp. 2246-2257.

Fujii, K. & Fujimoto, H. (2007). Traction control based on slip ratio estimation without detecting vehicle speed for electric vehicle, Proceeding of Fourth Power Conversion Conference-NAGOYA, pp.688-693.

Fujimoto, H.; Saito, T.; & Noguchi, T. (2004). Motion Stabilization Control of Electric Vehicle under Snowy Conditions Based on Yaw-Moment Observer, Proceeding of IEEE International Workshop on Advanced Motion Control 2004, pp.35-40.

Hori, Y. (2004). Future Vehicle Driven by Electricity and Control -Research on Four-Wheel-Motored "UOT Electric March II", IEEE Transaction on Industrial Electronics, Vol. 51, No. 5 pp. 954-962.

Ikeda M.; Ono T. & Aoki N. (1992). Dynamic mass measurement of moving vehicles, Transactions of the Society of Instrument and Control Engineers, Vol. 28, No. 1, pp. 50-58.

Lee, H. & Tomizuka, M. (2003). Adaptive Vehicle Traction Force Control for Intelligent Vehicle Highway Systems (IVHSs), IEEE Transaction on Industrial Electronics, Vol. 50, No. 1, pp. 37-47.

Mutoh, N.; Hayano, Y.; Yahagi, H. & Takita, K. (2007). Electric Braking Control Methods for Electric Vehicles With Independently Driven Front and Rear Wheels, IEEE Transaction on Industrial Electronics, Vol. 54, No. 2, pp.1168-1176.

Nagai, M. (2007). The perspectives of research for enhancing active safety based on advanced control technology, Vehicle System Dynamics, Vol. 45, No. 5, pp. 413-431.

Pacejka, H. B. & Bakker, E. (1992). The Magic Formula Tyre Model, Vehicle System Dynamics, Vol. 21, No. 1, pp. 1-18.

Ioannou P. A. & Sun J. (1995). Robust Adaptive Control, Prentice Hall, pp. 79-104.

Phornsuk, R. A.; Hiroshi, H.; Masatoshi, A. & Shigeto, O. (2006). Adaptive controller design for anti-slip system of EV, Procceding of 2006 IEEE Conference on Robotics, Automation and Mechatronics, No. 4018749.

Saito, T.; Fujimoto, H. & Noguchi, T. (2002). Yaw-Moment Stabilization Control of Small Electric Vehicle, Procceding of Industrial Instrumentation and Control, IEE Japan, pp. 83-88.

Sakai, S. & Hori, Y. (2001). Advantage of Electric motor for anti skid control of electric vehicle, European Power Electronics Journal, vol. 11, No. 4, pp. 26-32.

Sakai, S.; Sado, H. & Hori, Y. (1999). Motion Control in an Electric Vehicle with 4 Independently Driven In-Wheel Motors, IEEE Transaction on Mechatronics, vol.4, No.1, pp. 9-16.

Suryanarayanan, S. & Tomizuka, M. (2007). Appropriate Sensor Placement for Fault-Tolerant Lane-Keeping Control of Automated Vehicles, IEEE/ASME Transactions on Mechatronics, Vol. 12, No. 4, pp. 465-471.

Turner, J. D. & Austin, L. (2000). Sensors for Automotive Telematics, Measurement Science & Technology, Vol. 11, No. 2, pp. 58-79.

Winstead, V. & Kolmanovsky, I. V. (2005). Estimation of Road Grade and Vehicle Mass via Model PredictiveControl, Proceeding of IEEE Conference on Control Applications 2005, WC2.3.

Yin, D.; Oh, S.; & Hori, Y. (2009). A Novel Traction Control for EV Based on Maximum Transmissible Torque Estimation, IEEE Transaction on Industrial Electronics, Vol. 56, No. 6, pp. 2086-2094.

Motion Control

Edited by Federico Casolo

ISBN 978-953-7619-55-8
Hard cover, 590 pages
Publisher InTech
Published online 01, January, 2010
Published in print edition January, 2010

The book reveals many different aspects of motion control and a wide multiplicity of approaches to the problem as well. Despite the number of examples, however, this volume is not meant to be exhaustive: it intends to offer some original insights for all researchers who will hopefully make their experience available for a forthcoming publication on the subject.

INTECH
open science | open minds

InTech Europe
University Campus STeP Ri
Slavka Krautzeka 83/A
51000 Rijeka, Croatia
Phone: +385 (51) 770 447
Fax: +385 (51) 686 166
www.intechopen.com

InTech China
Unit 405, Office Block, Hotel Equatorial Shanghai
No.65, Yan An Road (West), Shanghai, 200040, China
中国上海市延安西路65号上海国际贵都大饭店办公楼405单元
Phone: +86-21-62489820
Fax: +86-21-62489821